Journal of Sound and Vibration (1997) **200**(4), 467–489

A UNIFIED BOUNDARY INTEGRAL METHODOLOGY FOR AERODYNAMICS AND AEROACOUSTICS OF ROTORS

M. Gennaretti, L. Luceri and L. Morino

Dipartimento di Meccanica e Automatica, *University of Rome III*, *via Corrado Segre*, 60 00146 *Roma*, *Italy*

(*Received* 19 *August* 1994, *and in final form* 5 *August* 1996)

A unified, potential-flow, boundary-integral formulation is presented for studying velocity and pressure fields around rotors in hover and forward flight, thereby providing a tool for an integrated analysis of aerodynamics and aeroacoustics in linear as well as non-linear problems. The integral formulation for aerodynamics, based on the assumption of potential flows, has been widely used by the authors in the past and has been validated extensively; the integral formulation for aeroacoustics, closely related to the aerodynamic one, yields the pressure in the field. Specifically, a boundary-integral equation allows one to evaluate the potential distribution around the body; after having obtained this, the corresponding boundary integral representation is used to evaluate the potential and hence the pressure at any point in the field. Numerical aerodynamic and aeroacoustic results, obtained with the proposed formulation for helicopter rotors in hover and forward flight at subsonic speeds, are in good agreement with experimental data and existing numerical results.

1. INTRODUCTION

This work deals with a boundary integral formulation for the unified analysis of aerodynamics and aeroacoustics of rotors in hover and forward flight. The formulation is based on a potential-flow assumption (specifically, it is assumed that the flow is quasi-potential, in the sense indicated in the next section). The integral formulation for aerodynamics has been widely used and extensively validated by the authors in the past (see below). Thus, the emphasis here is on the interplay between aerodynamics and aeroacoustics and the novel application of the aerodynamic formulation to aeroacoustic analysis.

In aerodynamics, the primary unknown is the pressure distribution over the surface of the body. This may be obtained computationally by using several numerical methods (e.g., finite differences, finite volumes, finite elements, boundary elements, and spectral methods). Here, the focus is on the boundary-element (or boundary-integral) approach, which involves the solution of a boundary integral equation, obtained in the limit, from the corresponding boundary integral representation, as the field point approaches the boundary surface (see section 3).

In aeroacoustics, the primary unknown is the pressure field away from the body. There exist two classical approaches used in aeroacoustics: (a) the Ffowcs Williams and Hawkings equation (see, e.g. references [1–3]) and (b) the Kirchhoff-surface approach (see, e.g., references [3–5]). In the first case, the pressure is obtained from a boundary integral representation giving the acoustic pressure in the field in terms of (i) geometry and motion

0022–460X/97/090467 + 23 $25.00/0/sv960713

of the surface of the body, (ii) the pressure acting on it, and (iii) the quadrupole term in the field, if non-linear effects are included. In the second case, the pressure is obtained from a boundary integral representation (Kirchhoff's formula for the wave equation and its extension to moving surfaces), which gives the pressure in the field in terms of the pressure and its normal derivative on a surface that surrounds the body and surrounds the non-linear term region. It may be noted that in both cases all the necessary aerodynamic input data are assumed to be known from the aerodynamic analysis. Thus, in acoustics, the operator is always linear; the non-linear analysis is always shifted to the aerodynamic analysis. The aerodynamic data may be obtained either from experimental data or from computational results. In this second case, the output of an aerodynamic code is the input for the aeroacoustic one; this provides a strong motivation for attempting an integration of aerodynamics and aeroacoustics.

A unified approach for aerodynamics and aeroacoustics of potential flows has been presented by Hanson [6, 7] for the frequency domain analysis of propellers, and by Long [8, 9], Farassat [10, 11], and Farassat and Myers [12] for the time domain analysis of bodies in arbitrary motion. All the unified aerodynamic/aeroacoustic formulations mentioned above derive a boundary integral equation for the pressure distribution on the body, starting from the linear form of the Ffowcs Williams and Hawkings equation [1].

It must be noted that the Ffowcs Williams and Hawkings equation is valid for viscous, compressible flows. For linear problems, this equation may be used to solve the aerodynamic problem, since there exists only one unknown variable (the acoustic pressure). However, this is not true for non-linear problems and thus the formulation based on the Ffowcs Williams and Hawkings equation may not be used for a non-linear aerodynamic analysis. The problem disappears if we limit ourselves to potential flows, since in this case one may use a formulation based on the velocity potential, φ, for which there exists an exact non-linear formulation in which the only unknown is φ (see section 2). This is the approach presented here. Specifically for the aeroacoustic analysis, the very same integral representation used (as an integral equation) for the aerodynamic one is utilized. This yields the potential in the field and hence the pressure, via Bernoulli's theorem.

The aerodynamic formulation addressed here stems from a general boundary-integral-equation formulation for the study of unsteady compressible potential aerodynamics introduced by Morino [13]. In that work, the integral equation is formulated in terms of the velocity potential and the formulation is valid for a surface undergoing arbitrary motion with respect to a body frame of reference which is in uniform translation with respect to the undisturbed air. For linear problems, the integral equation yields the velocity potential from the normal component of the velocity on the body, which is known from the boundary conditions, and the potential discontinuity across the wake known from the preceding time history. For non-linear (transonic) flows, the solution depends also upon the non-linear terms in the field. The formulation was further developed and has been validated for the case of airplanes at subsonic, transonic, and supersonic speeds. Given the scope of this paper, a review of the development of boundary integral formulations for potential aerodynamics is not attempted here: for this, the reader is referred to the paper by Morino and Tseng [14], Morino and Gennaretti [15], and Morino [16]. It suffices to say that the formulation for frames of reference in arbitrary motion used here is an evolution of past work of the authors ([17–22]).

Similarly, a review of the development of boundary integral formulations for aeroacoustics is not attempted here; extensive presentations of several aeroacoustic formulations have been given in Lyrintzis [4], and Brentner and Farassat [23]. The present boundary integral formulation is closely related to those commonly used in aeroacoustics for the evaluation of the acoustic field. The novelty is in the fact that, as mentioned above,

the unknown is the velocity potential, instead of the acoustic pressure or related quantities. On the other hand, the type of integral equation that is used is fully equivalent to those developed by Lighthill [24], Ffowcs Williams and Hawkings [1], and Farassat [2]. Indeed, in reference [21], a more general boundary integral representation is presented, which includes as particular cases the one presented here and those of Ffowcs Williams and Hawkings [1] and Farassat [2].

It should be emphasized that the numerical validation presented here is limited to subsonic flows with negligible BVI effects (the BVI effects require a free-wake analysis which is not included in the present results; however, the formulation itself does not preclude such possibility; see e.g., reference [17]). Thus, the emphasis in this paper is on the linear analysis. However, one important motivation for this work is the possibility of extending the approach to non-linear problems (for which preliminary numerical results exist, as indicated later in this section). Because the formulation is fully non-linear, it may be used for the solution of two important problems in rotor aerodynamics/aeroacoustics: (i) the analysis of rotors in transonic flow regimes, where non-negligible non-linear terms appear in the differential equation for the potential (preliminary numerical aerodynamic-aeroacoustic results for transonic rotors in hover have been presented by Gennaretti, Iemma and Morino [25]), and (ii) the analysis of configurations where BVI effects occur, in which the evaluation of the highly distorted wake geometry is required (for free-wake analysis results in incompressible flow; see reference [17]). Therefore, the fully non-linear differential formulation for the potential is outlined, but only to the extent necessary to illustrate the above point.

Specifically, the exact (non-linear) differential formulation for potential aerodynamics and aeroacoustics is presented in section 2. The boundary-integral formulation for the linearized problem is presented in section 3. In order to validate the formulation, in section 4 the present aerodynamic and aeroacoustic results are compared with existing experimental and numerical results for rotors in hover and forward flight in subsonic flows with moderate BVI effects.

Finally, concluding remarks are given in section 5. This paper is based on the doctoral thesis of Gennaretti [22]; the theoretical formulation was jointly developed by Gennaretti and Morino; Gennaretti and Luceri are responsible for the numerical validation.

2. FORMULATION FOR QUASI-POTENTIAL FLOWS

It is known that the forces acting on an object in steady potential flows are zero (d'Alembert paradox). This problem is resolved by allowing the flow to have a discontinuity on the potential (which implies the existence of a vortex layer in the field). In order to emphasize this fact, those flows which are potential everywhere except on zero thickness layers are here denoted by "quasi-potential" (this terminology is inspired by Chorin and Marsden [26], who define as "almost potential" those flows that are potential outside thin layers).

The formulation for quasi-potential flows (in particular, the issue of potential flow wakes and the corresponding boundary conditions) is not necessarily well known to the aeroacoustics community, where the formulation is usually cast in terms of acoustic pressure. Thus, for the sake of clarity and completeness, and in order to show the capability of the approach presented to provide a unified aerodynamic/aeroacoustic formulation also for non-linear problems, in this section the differential formulation for compressible quasi-potential flows, including all the non-linear terms that appear in the formulation, is outlined. The assumptions for a theory of compressible quasi-potential flows are that the flow be inviscid, non-conducting, shock-free, as well as initially homentropic and initially

irrotational (e.g., initially in dynamic and thermodynamic equilibrium). These assumptions are introduced below, as necessary.

The governing equations for inviscid, non-conducting, shock-free flows are the continuity equation, the Euler equation, and the entropy-evolution equation, $\mathrm{D}S/\mathrm{D}t = 0$ (where $\mathrm{D}/\mathrm{D}t$ denotes the substantial derivative). This last equation, combined with the assumptions of initially homentropic flow, implies that the flow is isentropic (i.e., homentropic at all times). Therefore, the relationship $\mathrm{d}h = \mathrm{d}p/\rho + T\,\mathrm{d}S$ (with h denoting the enthalpy) reduces to $\mathrm{d}h = \mathrm{d}p/\rho$. Hence, for compressible inviscid isentropic flows the acceleration is irrotational and Kelvin's theorem is valid. Thus, the assumption of initially irrotational flow implies that the flow remains irrotational at all times, except for the points of the wake to which Kelvin's theorem in not applicable (see section 2.2). Therefore, except for the wake points, the velocity may be expressed in terms of the velocity potential, φ, as $\mathbf{v} = \nabla\varphi$. As a consequence, excluding the wake points, the Euler equation has a first integral, i.e., Bernoulli's theorem which, in the frame of reference connected with the undisturbed air (air frame), where $\mathbf{v}_\infty = 0$, reads

$$\partial\varphi/\partial t + \tfrac{1}{2}v^2 + h = h_\infty, \tag{1}$$

with $v = \|\mathbf{v}\|$.

2.1. DIFFERENTIAL EQUATION FOR VELOCITY POTENTIAL

Note that for isentropic flows $\rho = \rho(p)$ and $\mathrm{d}p/\rho = \mathrm{d}h$: hence, the continuity equation, $\rho\nabla\cdot\mathbf{v} + \mathrm{D}\rho/\mathrm{D}t = 0$, may be written as $\nabla^2\varphi + a^{-2}\,\mathrm{D}h/\mathrm{D}t = 0$, where $a^2 = (\partial p/\partial\rho)|_S$. Combining this with equation (1) yields

$$\nabla^2\varphi = (1/a^2)/(\mathrm{D}/\mathrm{D}t)(\partial\varphi/\partial t + \tfrac{1}{2}v^2). \tag{2}$$

Equation (2) contains two unknowns, φ and a. A relationship between a and φ exists if the air is assumed to be an ideal gas with a constant specific heat coefficient. In this case, one has $h = \gamma p/(\gamma-1)\rho$ and $p/p_\infty = (\rho/\rho_\infty)^\gamma$, where γ denotes the specific heat ratio (isentropic law); hence, $a^2 = \gamma p/\rho = (\gamma-1)h$. Thus, Bernoulli's theorem yields $a^2 = c^2 - (\gamma-1)(\dot\varphi + v^2/2)$, where $c = a_\infty$ denotes the undisturbed speed of sound and $\dot\varphi = \partial\varphi/\partial t$. Eliminating a between this equation and equation (2) one obtains a differential equation in which the only unknown is the velocity potential, φ. This equation may be rewritten in a form suitable for a boundary integral formulation, by moving all the linear terms to the left side of the equation and all the non-linear terms to the right side. This yields

$$-\Box^2\varphi = \nabla^2\varphi - (1/c^2)/(\partial^2\varphi/\partial t^2) = \sigma, \tag{3}$$

where $\sigma = [(c^2 - a^2)\nabla^2\varphi + 2\mathbf{v}\cdot\dot{\mathbf{v}} + \mathbf{v}\cdot\nabla v^2/2]/c^2$ denotes all the non-linear terms, which are important only in the transonic region (and hence neglected in the following sections).

2.2. BOUNDARY CONDITIONS

In order to complete the problem, the boundary conditions are needed. In the air frame of reference used here, the boundary condition at infinity is given by $\varphi = 0$. Also, as to the presence of a body, it is typically assumed that its surface, $\mathscr{S}_B$ be impermeable; hence, the boundary condition on a point of $\mathscr{S}_B$ is $(\mathbf{v} - \mathbf{v}_B)\cdot\mathbf{n} = 0$, or

$$\partial\varphi/\partial n = \mathbf{v}_B\cdot\mathbf{n}, \quad \mathbf{x}\in\mathscr{S}_B, \tag{4}$$

where $\mathbf{v}_B$ is the velocity of the point $\mathbf{x}$ on the surface of the body $\mathscr{S}_B$ (more general boundary conditions, such as prescribed through-flow at a nacelle inlet, may be implemented by

adding the flux-term on the right side of equation (4); a similar term arises if one uses the transpiration-velocity formulation by Lighthill [27] to include the boundary-layer effects).

In addition, for quasi-potential flows, the issue of the wake and trailing-edge boundary conditions needs to be addressed. A detailed analysis of this is given in references [14–16]. Here, it suffices to note that the proof that an inviscid isentropic initially irrotational flow remains irrotational at all times fails for the fluid points that come in contact with the surface of the body, because Kelvin's theorem is not applicable in this case (since contours surrounding these points do not remain in the fluid volume at all times). These points form a surface called the wake which, in general, is a surface of discontinuity for the potential. There exist two types of surfaces of discontinuity, shock waves and wakes; wakes are defined as surfaces of discontinuity in which $\Delta v_N = 0$ (where $v_N = \mathbf{v} \cdot \mathbf{n}$ is the component of the velocity normal to the surface of discontinuity and $\Delta f = f_2 - f_1$ indicates the discontinuity across the surface), whereas shock waves are defined to be surfaces of discontinuity in which $\Delta v_N \neq 0$. Hence, the boundary conditions for the wake may be obtained from the conservation principles across a surface of discontinuity. Combining the principle of conservation of mass, $\Delta[\rho(v_N - v_W)] = 0$ (where v_W is the speed of the wake surface, by definition in the direction of the normal $\mathbf{n}$), with $\Delta v_N = 0$ yields $\Delta\rho = 0$. Also, the principle of conservation of momentum, $\Delta[\rho(v_N - v_W)\mathbf{v} + p\mathbf{n}] = 0$, yields

$$\Delta p = 0 \tag{5}$$

and $\rho(v_N - v_W)\Delta\mathbf{v} = 0$. Since $\Delta\mathbf{v} \neq 0$ (otherwise there exists no discontinuity at all), one obtains $v_N = v_W$, which indicates that the fluid does not penetrate the surface of the wake. This fact implies that the above result of isentropic flow is valid as well in the presence of the wake (alternatively, $\Delta\rho = 0$ and $\Delta p = 0$ imply $\Delta S = 0$). Hence, repeating the considerations presented above, one obtains that the flow remains irrotational everywhere except for the wake points.

Next, consider the wake boundary conditions for quasi-potential flows; $\Delta v_N = 0$ implies

$$\Delta(\partial\varphi/\partial n) = 0. \tag{6}$$

In order to obtain a boundary condition for the potential discontinuity $\Delta\varphi$, one notes that $\Delta\rho = 0$ and $\Delta p = 0$ imply $\Delta h = 0$. Combining this with Bernoulli's theorem (equation (1)), one obtains $\dot{\varphi}_2 - \dot{\varphi}_1 + (v_2^2 - v_1^2)/2 = 0$, where 1 and 2 denote the two sides of the wake. Then, noting that $v_2^2 - v_1^2 = (\mathbf{v}_2 + \mathbf{v}_1) \cdot (\mathbf{v}_2 - \mathbf{v}_1)$, one has

$$(\mathrm{D}_W/\mathrm{D}t)\Delta\varphi = 0, \tag{7}$$

where $\mathrm{D}_W/\mathrm{D}t = \partial/\partial t + \mathbf{v}_W \cdot \nabla$ denotes the substantial derivative following a wake point $\mathbf{x}_W$, which is defined as a point having velocity $\mathbf{v}_W = (\mathbf{v}_1 + \mathbf{v}_2)/2$. Equation (7) is the desired evolution equation for $\Delta\varphi$ and implies that $\Delta\varphi$ remains constant following a wake point $\mathbf{x}_W$, and equal to the value it had when $\mathbf{x}_W$ left the trailing edge. This value may be obtained by imposing that concentrated vortices do not exist at the trailing edge; the implication of this assumption is that

$$\lim_{\mathbf{x}_2 \to \mathbf{x}_{TE}} \varphi - \lim_{\mathbf{x}_1 \to \mathbf{x}_{TE}} \varphi = \lim_{\mathbf{x}_W \to \mathbf{x}_{TE}} \Delta\varphi, \tag{8}$$

where $\mathbf{x}_1$ and $\mathbf{x}_2$ are two points on opposite sides of the body surface (see reference [16] for a more detailed discussion of this point).

Finally, it should be noted that, for quasi-potential flows, the above formulation governs both aerodynamic and aeroacoustics: indeed, in both cases the objective of the analysis is the evaluation of the pressure (on the boundary surface in aerodynamics and in the field in aeroacoustics). It should also be emphasized that the above formulation (exact, in that

all the non-linear effects are included) is cast in terms of only one unknown, the velocity potential. As mentioned above, the same is not true for the formulation in terms of the acoustic pressure, because in this case, even for potential flows, the non-linear terms depends both on the acoustic pressure and on the velocity field (see, e.g., the expression of the Lighthill stress tensor in reference [24]).

3. BOUNDARY INTEGRAL FORMULATION

In this section the boundary integral formulation for the solution of the velocity potential field is presented, when the fluid is perturbed by the presence of a lifting body in arbitrary rigid-body motion. One assumes that the flow remains subsonic at all times and that the non-linear term σ in equation (3) is negligible. Hence, the solution is determined from the homogeneous wave equation for the potential.

Now consider two disjoint closed rigid surfaces $\mathscr{S}_B$ and $\mathscr{S}'_W$ surrounding, respectively, the volume $\mathscr{D}_B$ occupied by the body and the volume $\mathscr{D}_W$ occupied by a thin fluid region containing the wake surface, $\mathscr{S}_W$, (see Figure 1), which is assumed to be time independent in an appropriate frame of reference (e.g., the rotor frame for the hover case, or the air frame in the forward case, see section 3.2).

In order to derive an integral representation for the linear form of equation (3), it is convenient to recast it into an equivalent infinite-space problem. To this end, a domain function $E(\mathbf{x}, t)$ is introduced, defined as $E = 1$ in $\mathscr{V} = \mathbb{R}^3 \backslash \mathscr{D}$, where $\mathscr{D} = \mathscr{D}_B \cup \mathscr{D}_W$, and $E = 0$ otherwise. Consider also the function $\hat{\varphi}(\mathbf{x}, t) = E(\mathbf{x}, t)\varphi(\mathbf{x}, t)$. Then, the original problem (equation 3), with $\sigma = 0$, may be replaced by the following infinite-space problem:

$$-\Box^2\hat{\varphi} = \nabla E \cdot \nabla\varphi + \nabla \cdot (\varphi \nabla E) - \frac{1}{c^2}\left[\frac{\partial E}{\partial t}\frac{\partial \varphi}{\partial t} + \frac{\partial}{\partial t}\left(\varphi \frac{\partial E}{\partial t}\right)\right]. \tag{9}$$

Upon applying the boundary integral method, the formal solution of equation (9) is found to be

$$E(\mathbf{x}, t)\varphi(\mathbf{x}, t) = \int_{-\infty}^{\infty}\int_{\mathbb{R}^3} G\nabla E \cdot \nabla\varphi \, \mathrm{d}\mathbf{y} \, \mathrm{d}\tau + \int_{-\infty}^{\infty}\int_{\mathbb{R}^3} \nabla \cdot (\varphi \nabla E) G \, \mathrm{d}\mathbf{y} \, \mathrm{d}\tau$$

$$-\frac{1}{c^2}\int_{-\infty}^{\infty}\int_{\mathbb{R}^3} G\frac{\partial E}{\partial \tau}\frac{\partial \varphi}{\partial \tau} \, \mathrm{d}\mathbf{y} \, \mathrm{d}\tau - \frac{1}{c^2}\int_{-\infty}^{\infty}\int_{\mathbb{R}^3} \frac{\partial}{\partial \tau}\left(\varphi \frac{\partial E}{\partial \tau}\right) G \, \mathrm{d}\mathbf{y} \, \mathrm{d}\tau, \tag{10}$$

where G is the fundamental solution of the wave equation, given by

$$G(\mathbf{y} - \mathbf{x}, \tau - t) = (-1/4\pi r)\delta(\tau - t + r/c), \tag{11}$$

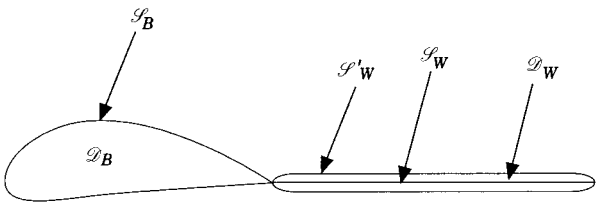

Figure 1. 2-D sketch representing body surface, $\mathscr{S}_B$, body volume, $\mathscr{D}_B$, wake surface, $\mathscr{S}_W$, and surface $\mathscr{S}'_W$ surrounding the volume $\mathscr{D}_W$ occupied by a thin fluid region containing the wake.

where $r = \|\mathbf{y} - \mathbf{x}\|$, δ denotes the Dirac delta function, and $\mathbf{x}$ and t are observer location and time in the air frame of reference, whereas $\mathbf{y}$ and τ are source location and time also in the air frame of reference.

Next, note that the integrals in equation (10) contain two Dirac delta functions, one stemming from the derivatives of E, and the other from the expression for G. In order to perform the integrations, note that $\mathscr{D}_B \cap \mathscr{D}_W = \emptyset$ implies $E = E_B E_W$, where $E_B = 1$ in $\mathbb{R}^3 \backslash \mathscr{D}_B$ and $E_B = 0$ in $\mathscr{D}_B$ (similarly for the wake); hence, using properties of the Dirac delta function, one has $\nabla E = \nabla E_B + \nabla E_W$ and $\partial E/\partial t = \partial E_B/\partial t + \partial E_W/\partial t$. Thus, the contributions from body and wake decouple and equation (10) may be written in the symbolic form

$$E(\mathbf{x}, t)\varphi(\mathbf{x}, t) = I_B + I_W, \tag{12}$$

where I_B and I_W represent integral contributions of the body and wake surface, respectively.

Thus, each contribution may be evaluated in the most convenient frame of reference. For instance, for I_B one may choose a frame of reference fixed with the body volume, $\mathscr{D}_B$, where E_B is not a function of time.

3.1. BODY CONTRIBUTION

In order to derive an expression for the integral contributions from the body that is more suitable for applications, let $\check{\mathbf{x}}$ and $\check{t}$ (with $\check{t} \equiv t$) denote space and time variables in the space rigidly connected with $\mathscr{D}_B$ (body space), and let $\mathbf{x} = \hat{\mathbf{x}}(\check{\mathbf{x}}, \check{t})$ be the transformation relating the two spaces.

Then, observe that for any differentiable function f, one has

$$\partial/\partial t = \partial/\partial \check{t} - \mathbf{v}_R \cdot \nabla := \mathrm{d}/\mathrm{d}\check{t}, \tag{13}$$

where $\mathbf{v}_R(\check{\mathbf{x}}, \check{t}) = \partial \hat{\mathbf{x}}(\check{\mathbf{x}}, \check{t})/\partial \check{t}$ denotes the velocity of a point $\check{\mathbf{x}}$ of the body space with respect to air space.

Next, recall that, for any h and g,

$$\int_{-\infty}^{\infty} h(t)\delta[g(t)]\,\mathrm{d}t = \sum_k \left[\frac{h(t)}{|\dot{g}(t)|}\right]_{t=t_k} = \sum_k \int_{-\infty}^{\infty} \frac{h(t)}{|\dot{g}(t)|}\,\delta(t - t_k)\,\mathrm{d}t, \tag{14}$$

where t_k are the roots of $g(t) = 0$. In our case, from equation (11) one has, in the body space, $g = g(\check{\tau}) = \check{\tau} - \check{t} + \|\hat{\mathbf{x}}(\check{\mathbf{y}}, \check{\tau}) - \hat{\mathbf{x}}(\check{\mathbf{x}}, \check{t})\|/c$, and hence $\dot{g} = 1 + M_r$, with $M_r = \mathbf{r} \cdot \mathbf{v}_R / rc$, where $\mathbf{r} = \hat{\mathbf{x}}(\check{\mathbf{y}}, \check{\tau}) - \hat{\mathbf{x}}(\check{\mathbf{x}}, \check{t})$ (akin to the air frame of reference, $\check{\mathbf{y}}$ and $\check{\tau}$ denote source location and time in the body frame of reference).

As mentioned above, here the cases are limited to subsonic flow, and hence the equation $g = 0$ has only one root, which one denotes with $\check{t} - \theta$. Thus, combining the above expressions with equation (10) and performing an integration by parts over the second and fourth integral on the right hand side (with $\varphi = 0$ at infinity and zero initial conditions), and taking advantage of the fact that $\nabla \cdot \mathbf{v}_R = 0$ (since $\mathbf{v}_R$ is the velocity of a point of the body space with respect to the undisturbed air, i.e., a velocity corresponding to a rigid-body motion), one obtains

$$I_B(\check{\mathbf{x}}, \check{t}) = \int_{-\infty}^{\infty} \int_{\mathbb{R}^3} \check{G} \nabla E_B \cdot \nabla \varphi \,\mathrm{d}\check{\mathbf{y}}\,\mathrm{d}\check{\tau} - \int_{-\infty}^{\infty} \int_{\mathbb{R}^3} \varphi \nabla E_B \cdot \nabla \check{G}\,\mathrm{d}\check{\mathbf{y}}\,\mathrm{d}\check{\tau}$$

$$- \frac{1}{c^2} \int_{-\infty}^{\infty} \int_{\mathbb{R}^3} \check{G} \frac{\mathrm{d}E_B}{\mathrm{d}\check{\tau}} \frac{\mathrm{d}\varphi}{\mathrm{d}\check{\tau}}\,\mathrm{d}\check{\mathbf{y}}\,\mathrm{d}\check{\tau} + \frac{1}{c^2} \int_{-\infty}^{\infty} \int_{\mathbb{R}^3} \varphi \frac{\mathrm{d}E_B}{\mathrm{d}\check{\tau}} \frac{\mathrm{d}\check{G}}{\mathrm{d}\check{\tau}}\,\mathrm{d}\check{\mathbf{y}}\,\mathrm{d}\check{\tau}, \tag{15}$$

where

$$\check{G}(\check{\mathbf{y}}, \check{\mathbf{x}}, \check{\tau}, \check{t}) = \check{G}_0 \delta(\check{\tau} - \check{t} + \theta), \tag{16}$$

with

$$\check{G}_0 = (-1/4\pi)[1/r|1 + M_r|]_{\check{t} = \check{t} - \theta}. \tag{17}$$

Next, note that

$$\nabla \check{G} = \nabla \check{G}_0 \delta(\check{\tau} - \check{t} + \theta) + \check{G}_0 \dot{\delta}(\check{\tau} - \check{t} + \theta) \nabla \theta \tag{18}$$

and

$$\partial \check{G} / \partial \check{\tau} = \check{G}_0 \dot{\delta}(\check{\tau} - \check{t} + \theta). \tag{19}$$

Also, note that if (as in the present case) $\mathscr{D}_B$ is time independent, then $\partial E_B / \partial \check{t} = 0$. Hence, for any $\mathbf{a}(\check{\mathbf{x}}, \check{t})$,

$$\int_{-\infty}^{\infty} \int_{\mathbb{R}^3} \mathbf{a} \cdot \nabla E_B \delta[\check{t} - \check{t}_0(\check{\mathbf{x}})] \, \mathrm{d}\check{\mathbf{x}} \, \mathrm{d}\check{t} = \int_{\mathscr{S}_B} [\mathbf{a} \cdot \mathbf{n}]_{\check{t} = \check{t}_0} \, \mathrm{d}\mathscr{S}. \tag{20}$$

Furthermore, for any $f(\check{\mathbf{x}}, \check{t})$,

$$\int_{-\infty}^{\infty} \int_{\mathbb{R}^3} f \frac{\mathrm{d}E_B}{\mathrm{d}t} \, \delta[\check{t} - \check{t}_0(\check{\mathbf{x}})] \, \mathrm{d}\check{\mathbf{x}} \, \mathrm{d}\check{t} = -\int_{\mathscr{S}_B} [f \mathbf{v}_R \cdot \mathbf{n}]_{\check{t} = \check{t}_0} \, \mathrm{d}\mathscr{S}. \tag{21}$$

Hence, recalling that $\int_{-\infty}^{\infty} f(t) \dot{\delta}(t) \, \mathrm{d}t = -\dot{f}(0)$, and combining equations (18), (19), (20), and (21) with equation (15), one obtains

$$I_B(\check{\mathbf{x}}, \check{t}) = \int_{\mathscr{S}_B} \left[\frac{\partial \varphi}{\partial \tilde{n}} \check{G}_0 - \varphi \frac{\partial \check{G}_0}{\partial \tilde{n}} \right]_{\check{t} = \check{t} - \theta} \mathrm{d}\mathscr{S} + \int_{\mathscr{S}_B} \left[\check{G}_0 \frac{\partial \varphi}{\partial \check{\tau}} \left(\frac{\partial \theta}{\partial \tilde{n}} + 2 \frac{\mathbf{v}_R \cdot \mathbf{n}}{c^2} \right) \right]_{\check{t} = \check{t} - \theta} \mathrm{d}\mathscr{S}$$

$$+ \frac{1}{c^2} \int_{\mathscr{S}_B} \left[\varphi \check{G}_0 \frac{\partial}{\partial \check{\tau}} [\mathbf{v}_R \cdot \mathbf{n}(1 - \mathbf{v}_R \cdot \nabla \theta)] \right]_{\check{t} = \check{t} - \theta} \mathrm{d}\mathscr{S}, \tag{22}$$

where

$$\frac{\partial}{\partial \tilde{n}} = \frac{\partial}{\partial n} - \frac{1}{c^2} \mathbf{v}_R \cdot \mathbf{n} \, \mathbf{v}_R \cdot \nabla. \tag{23}$$

3.2. WAKE CONTRIBUTION

Note that for airplanes in uniform translation and for helicoptor rotors in hover, the wake surface may be assumed to be rigidly connected to the body. Whenever the wake may be assumed to be fixed in the body frame, the formulation (used here for the hover results) is relatively simple and is available in reference [14]; thus, for the sake of conciseness, it is not discussed here. Here, the formulation for rotors in forward flight is discussed, under the assumption that the motion of the wake surface with respect to the air frame of reference is negligible (this assumption is also acceptable for airplanes in maneuvering for which the present formulation is also applicable). (If this were not true (e.g., in configurations where the BVI occurs), one would use a generalization of the formulation to bodies that move in arbitrary (not rigid body) motion. The formulation for deforming surfaces has been examined by Morino [13] for translating frames of reference, and by Morino and Tseng [14] for frames of reference in

arbitrary motion. An extension of these formulations was introduced by Gennaretti [22] and is (i) compatible with the present formulation, (ii) applicable to N disjoint surfaces, and (iii) capable of dealing with a deforming wake in a frame of reference different from that of the corresponding blade.)

Under the assumption that the motion of the wake surface with respect to the air frame of reference is negligible, the volume $\mathscr{D}_W$ (see Figure 1) is fixed with respect to the air frame of reference and one obtains $\partial E_W/\partial t = 0$. Therefore, integrating by parts the second integral in equation (10), and observing again that $\varphi = 0$ at infinity, yields

$$I_W(\mathbf{x}, t) = -\int_{-\infty}^{\infty} \int_{\mathscr{S}'_W} \left(\frac{\partial \varphi}{\partial n} G - \varphi \frac{\partial G}{\partial n} \right) \mathrm{d}\mathscr{S}\, \mathrm{d}\tau, \tag{24}$$

where S'_W is the boundary of $\mathscr{D}_W$ (i.e., a closed surface that surrounds the open wake surface $\mathscr{S}_W$. Performing the limit as the two sides of $\mathscr{S}'_W$ approach the wake surface, $\mathscr{S}_W$, (see Figure 1) and using the first wake boundary condition, equation (6), one obtains

$$I_W(\mathbf{x}, t) = -\int_{-\infty}^{\infty} \int_{S_W} \Delta\varphi \frac{\partial G}{\partial n} \mathrm{d}\mathscr{S}\, \mathrm{d}\tau. \tag{25}$$

In order to perform the time integration, it is convenient to introduce a system of co-ordinates, λ and α, over the surface of the wake as defined below. Having assumed that the motion of the wake in the air frame of reference is negligible, one has that the wake surface coincides with that swept by the trailing edge during its motion. Hence, it is convenient (and legitimate) to identify one of the two co-ordinates with the arclength λ along the trailing edge (in other words, the lines $\lambda =$ constant identify the trajectory of a trailing-edge point). Also, it is natural to identify the other co-ordinate, α, with the time at which the trailing edge occupied that location. Next, consider the covariant base vectors of the above coordinate system, $\mathbf{a}_\lambda = \partial\mathbf{x}/\partial\lambda$ and $\mathbf{a}_\alpha = \partial\mathbf{x}/\partial\alpha$. Note that, because of the above choices made for the co-ordinates λ and α, $\mathbf{a}_\lambda = \partial\mathbf{x}/\partial\lambda$ is the unit tangent to the trailing edge at time $t = \alpha$, whereas $\mathbf{a}_\alpha = \partial\mathbf{x}/\partial\alpha$ is the velocity, $\mathbf{v}_{TE}$, of the trailing edge point, also at time $t = \alpha$. In this co-ordinate system, we have $\mathrm{d}\mathscr{S} = \sqrt{a}\, \mathrm{d}\alpha\, \mathrm{d}\lambda$ with $\sqrt{a} = \| \mathbf{a}_\alpha \times \mathbf{a}_\lambda \| = v_\nu$, where v_ν is the absolute value of the component of the velocity of the trailing edge point in the direction of $\boldsymbol{\nu}$ (normal to the trailing edge in the tangent plane of the wake).

Next, note that the wake surface grows progressively in time because of the sweeping motion of the trailing edge. Hence, because of the fact that in compressible flows a signal has a finite speed of propagation, a point $\mathbf{x}$ at time t will be influenced not by the entire wake surface already generated at time t, but only by the points $\mathbf{y}$ that were present at the retarded time $\tau = t - \theta$ (with θ a function of both $\mathbf{x}$ and $\mathbf{y}$). As shown later, this yields a line-integral contribution from the line separating the influencing and the non-influencing portion of the wake (see Figure 2). In order to show this, one starts by noting that in equation (24) the complete wake surface generated up to time t is included (including the non-influencing portion of the wake). Correspondingly, the doublet intensity must be defined as one which is equal to $\Delta\breve{\varphi}(\alpha, \lambda)$ on the portion of the wake already generated at time $\tau = t$, and equal to zero otherwise (note that $\Delta\breve{\varphi}$ is time independent because of equation (7)). In other words, noting that, by definition of α, the co-ordinate $\alpha_{TE}(t)$ of the trailing-edge at time t coincides with t, one has

$$\Delta\varphi(\alpha, \lambda, t) = \Delta\breve{\varphi}(\alpha, \lambda)\mathrm{H}(t - \alpha) \tag{26}$$

where H is the Heaviside function.

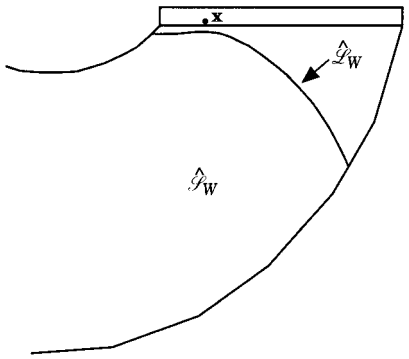

Figure 2. Surface of integration $\hat{\mathscr{S}}_W$ and line of integration $\hat{\mathscr{L}}_W$ on the wake, for a control point, **x**, placed on an advancing-rotor blade.

Combining equations (25) and (26), one has, setting $\alpha = t$,

$$
\begin{aligned}
I_W(\mathbf{x}, t) = &- \int_{-\infty}^{\infty} \int_{\lambda_1}^{\lambda_2} \Delta\check{\varphi} \mathrm{H}(f_1) \frac{\partial G_0}{\partial n} \delta(f_2) v_v \, \mathrm{d}\alpha' \, \mathrm{d}\lambda \, \mathrm{d}\tau \\
&- \int_{-\infty}^{\infty} \int_{\lambda_1}^{\lambda_2} \int_{0}^{\alpha} \Delta\check{\varphi} \mathrm{H}(f_1) G_0 \frac{\partial r}{\partial n} \dot{\delta}(f_2) \frac{v_v}{c} \, \mathrm{d}\alpha' \, \mathrm{d}\lambda \, \mathrm{d}\tau \\
= &- \int_{\lambda_1}^{\lambda_2} \int_{0}^{\alpha} \Delta\check{\varphi} \mathrm{H}(f_3) \frac{\partial G_0}{\partial n} v_v \, \mathrm{d}\alpha' \, \mathrm{d}\lambda \\
&+ \int_{-\infty}^{\infty} \int_{\lambda_1}^{\lambda_2} \int_{0}^{\alpha} \Delta\check{\varphi} \, \delta(f_1) G_0 \frac{\partial r}{\partial n} \delta(f_2) \frac{v_v}{c} \, \mathrm{d}\alpha' \, \mathrm{d}\lambda \, \mathrm{d}\tau,
\end{aligned} \tag{27}
$$

where $G_0 = -1/4\pi r, f_1 = \tau - \alpha', f_2 = \tau - t + r/c$ and $f_3 = f_1 - f_2 = t - r/c - \alpha'$, whereas λ_1 and λ_2 denote the extremes of the trailing edge.

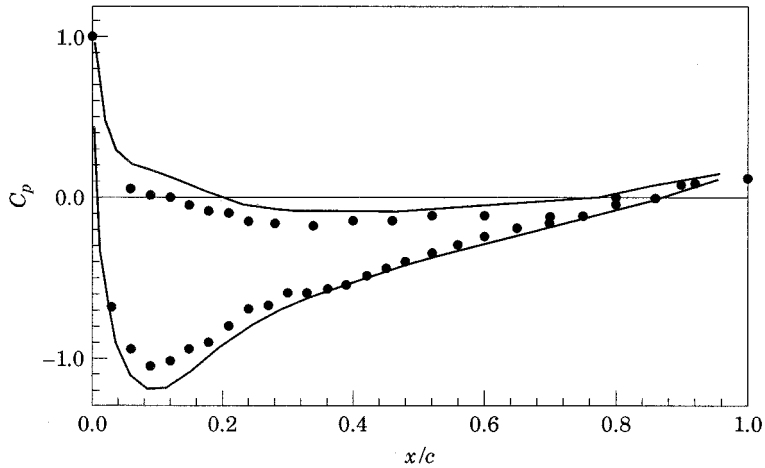

Figure 3. Pressure coefficient at section $r/R = 0{\cdot}75$ of the hovering BO-105 main rotor. ——, present results; ●, experimental results [28].

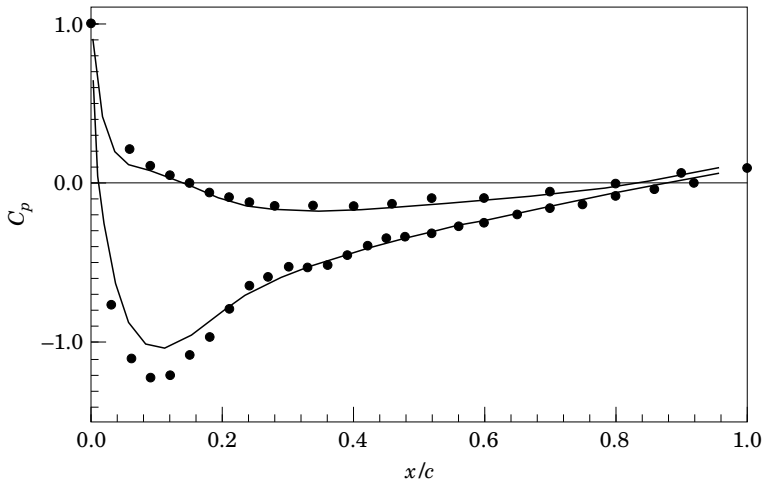

Figure 4. Pressure coefficient at section $r/R = 0{\cdot}97$ of the hovering BO-105 main rotor. ——, present results; ●, experimental results [28].

In order to evaluate the last integral it is convenient to integrate first with respect to τ. Then, the integration with respect to the variable α' is performed by using equation (14) with $g(\alpha') = \alpha' - t + r(\alpha')/c$. This yields

$$I_W(\mathbf{x}, t) = -\int_{\hat{\mathscr{S}}_W} \Delta\check{\varphi}\,\frac{\partial G_0}{\partial n}\,\mathrm{d}\mathscr{S} + \int_{\lambda_1}^{\lambda_2}\left[\Delta\check{\varphi}G_0\,\frac{1}{1+M_r}\,\frac{\partial r}{\partial n}\,\frac{v_v}{c}\right]_{\alpha'=\alpha_0}\mathrm{d}\lambda, \tag{28}$$

where $\hat{\mathscr{S}}_W$ is the portion of the wake influencing the potential at the point $\mathbf{x}$ at time t, whereas $\alpha_0(\lambda, \mathbf{x}, t)$ is defined implicitly by $g(\alpha_0) = 0$, and

$$1 + M_r = \partial g/\partial\alpha' = 1 + \mathbf{r}\cdot\mathbf{v}_{TE}/rc > 0. \tag{29}$$

In addition, the last integral is evaluated for $\alpha' = \alpha_0$: i.e., on line $\hat{\mathscr{L}}_W$ which separates the two regions of the wake (see Figure 2).

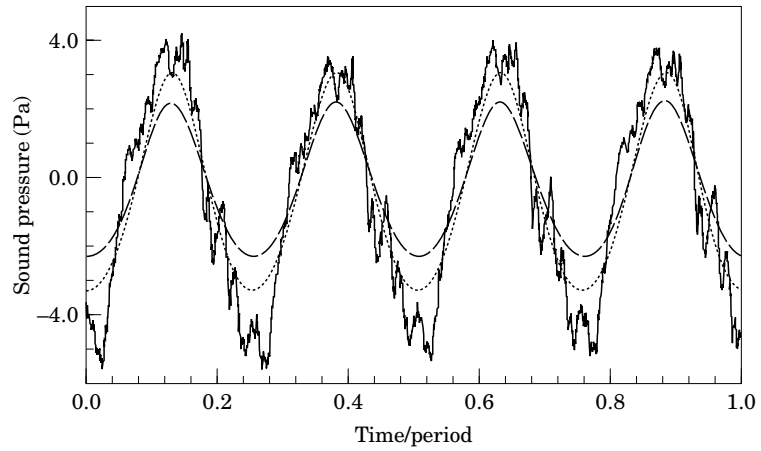

Figure 5. Acoustic signal of the hovering BO-105 main rotor, at observer located 2·3 m below the rotor disk and at a distance of 3·4 m from the rotor axis. - - - - -, present results with Landgrebe wake model; — — —, present results with helicoidal wake model; ——, experimental results [28].

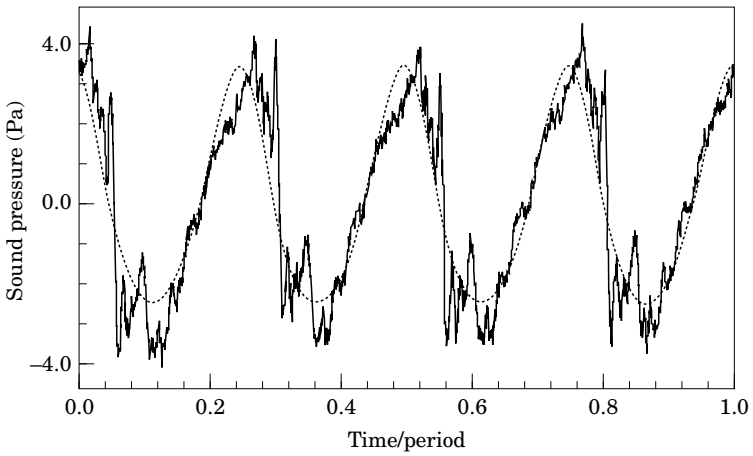

Figure 6. Acoustic signal of the hovering BO-105 main rotor, at observer located 2·3 m below the rotor disk and at a distance of 4·0 m from the rotor axis. - - - - -, present results; ——, experimental results [28].

3.3. SOLUTION PROCEDURE

Equation (12), with I_B expressed by equation (22) and I_W by equation (28) is the boundary integral representation (for the specific problem under consideration, i.e., rigid body with a wake fixed in the air space) for the solution to linearized equation (3) (with the initial conditions and infinity boundary condition defined above). If $\mathbf{x}$ tends to the boundary, equation (12) yields a compatibility condition that must be satisfied by the solution of the problem. In our case $\partial\varphi/\partial n$ is known from the boundary condition of impermeability of the body surface, and therefore such a compatibility condition is an integral equation for φ on the boundary. Once φ on the surface is known, φ and hence $\mathbf{v}$ may be evaluated anywhere in the field.

The numerical formulation utilized for the results is briefly outlined (for details on the discretization, see reference [15]). The body and wake surfaces are divided into quadrilateral elements and φ, $\partial\varphi/\partial\tilde{n}$, $\partial\varphi/\partial t$ and $\Delta\varphi$ are assumed to be constant within each element (zeroth order boundary element discretization). The resulting discretized equations

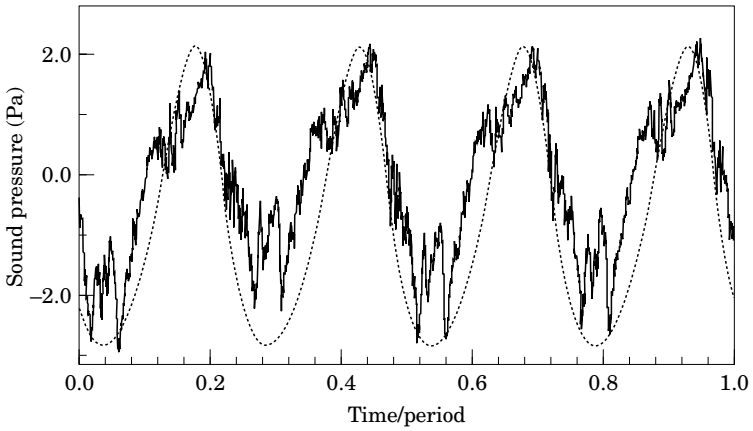

Figure 7. Acoustic signal of the hovering BO-105 main rotor, at observer located 2·3 m below the rotor disk and at a distance of 4·826 m from the rotor axis. - - - -, present results; ——, experimental results [28].

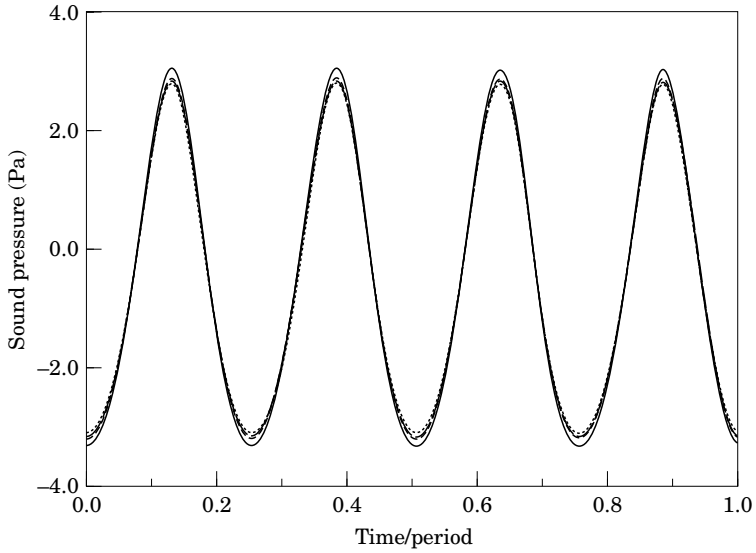

Figure 8. Convergence analysis for the acoustic signal of the hovering BO-105 main rotor, at observer located 2·3 m below the rotor disk and at a distance of 3·4 m from the rotor axis. - - - - -, $N = 2$; – – –, $N = 3$; — · — · —, $N = 4$; ——, $N \to \infty$.

are satisfied at the centers of the elements (collocation method). The equations are discretized in time (with piecewise linear interpolation). This yields a system of difference equations, the solution of which is obtained step by step. The pressure at the centers of the elements is evaluated from the solution of the potential field via the Bernoulli theorem, by applying a central finite difference algorithm for the evaluation of the tangential components of the velocity from the values of the potential, also at the centers of the elements. The acoustic pressure is obtained by first evaluating the potential at observer locations, and then applying the linearized Bernoulli theorem, with the velocity obtained by finite differences, from the potential evaluated at appropriate points in the neighbourhood of observer locations.

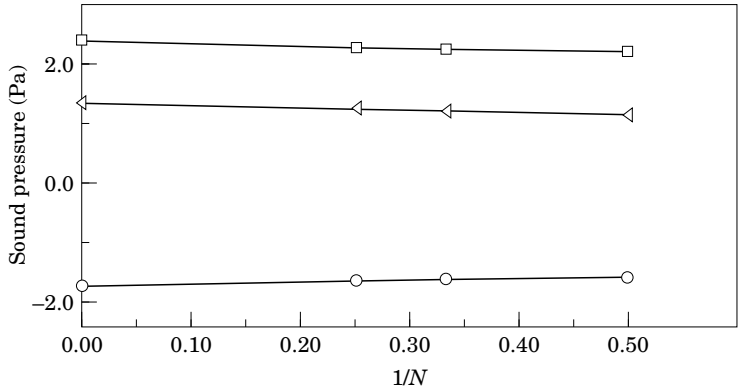

Figure 9. Convergence analysis for the acoustic signal of the hovering BO-105 main rotor, at observer located 2·3 m below the rotor disk and at a distance of 3·4 m from the rotor axis. Convergence rate of signals at three different times: ○, time/period = 0·056; □, time/period = 0·112, ◁, time/period = 0·168.

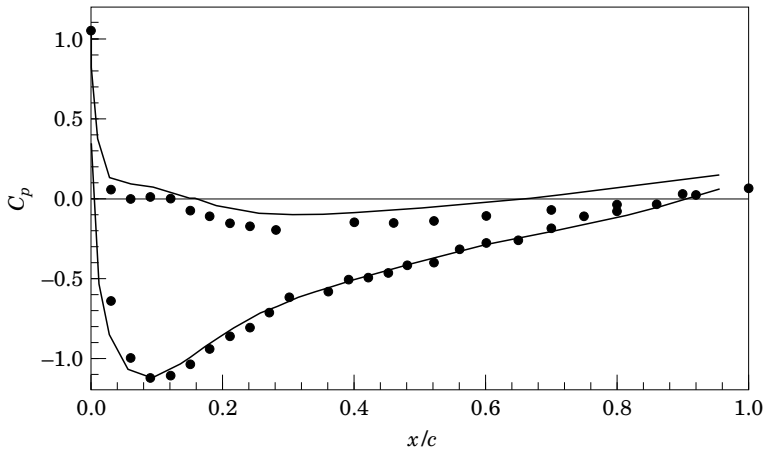

Figure 10. Pressure coefficient at section $r/R = 0{\cdot}75$ of the BO-105 main rotor at azimuthal position $\psi = 30^\circ$. ——, present results, ●, experimental results [28].

3.4. FORMULATION FOR MULTIPLE BODIES AND WAKES

It may be worth noting that the above formulation may be extended to the case on N disjoint bodies (e.g., a helicopter main-rotor/tail-rotor/fuselage configuration), each moving in arbitrary rigid-body motion, and M disjoint wake surfaces (each of which is rigid in a suitable frame of reference). In this case,

$$E = \prod_{n=1}^{N+M} E_n,$$

where

$$E_n(\mathbf{x}) = 0 \text{ if } \mathbf{x} \in \mathscr{D}_n, \text{ and } E_n(\mathbf{x}) = 1 \text{ otherwise.}$$

As mentioned above, the fact that the bodies are disjoint implies

$$\nabla E = \sum_{n=1}^{N+M} \nabla E_n \text{ and } \partial E/\partial t = \sum_{n=1}^{N+M} \partial E_n/\partial t.$$

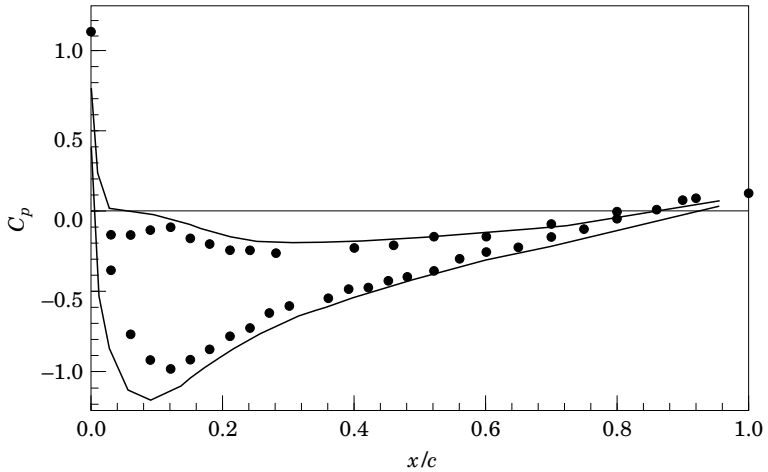

Figure 11. Pressure coefficient at section $r/R = 0{\cdot}75$ of the BO-105 main rotor at azimuthal position $\psi = 120^\circ$. ——, present results, ●, experimental results [28].

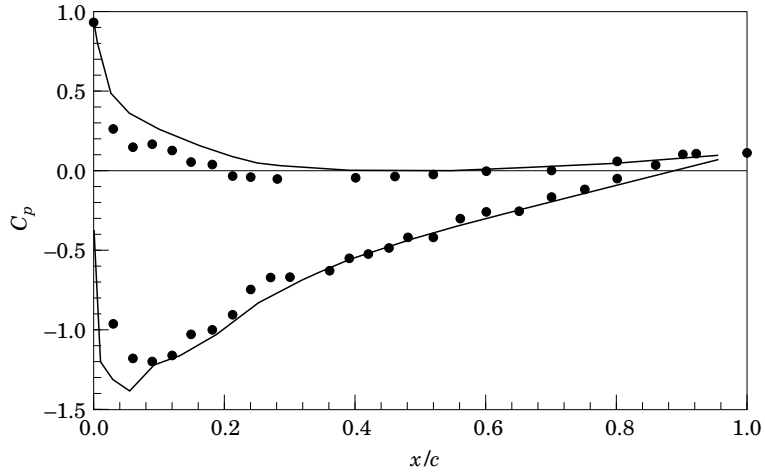

Figure 12. Pressure coefficient at section $r/R = 0{\cdot}75$ of the BO-105 main rotor at azimuthal position $\psi = 210^\circ$. ——, present results, ●, experimental results [28].

Thus, it is legitimate and convenient to evaluate each of these integrals in a frame of reference fixed with the corresponding body (or wake), since, in such a frame of reference, E_n is not a function of time. Thus, one has

$$E(\mathbf{x}, t)\varphi(\mathbf{x}, t) = \sum_{n=1}^{N+M} I_n, \tag{30}$$

where I_n denotes the integral contribution from the nth body or wake (each expressed in the most convenient frame of reference). As mentioned above, the formulation for non-rigid surfaces has been presented by Gennaretti [22].

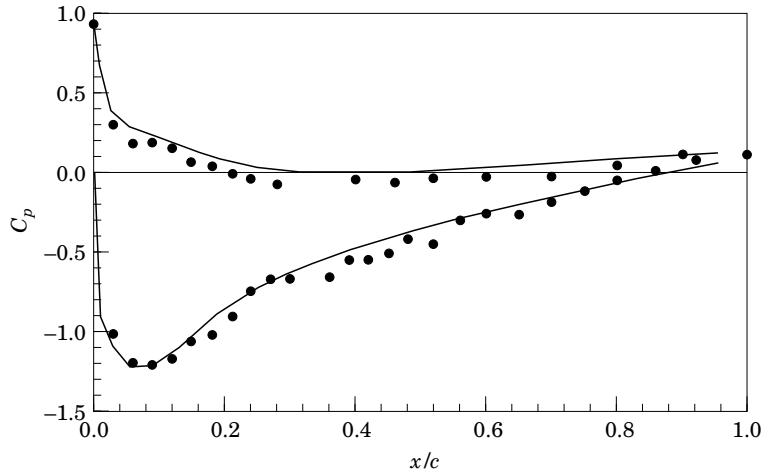

Figure 13. Pressure coefficient at section $r/R = 0{\cdot}75$ of the BO-105 main rotor at azimuthal position $\psi = 300^\circ$. ——, present results, ●, experimental results [28].

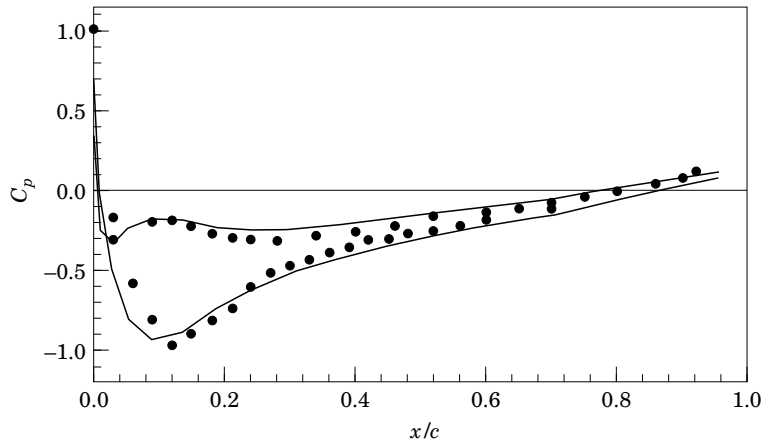

Figure 14. Pressure coefficient at section $r/R = 0{\cdot}97$ of the BO-105 main rotor at azimuthal position $\psi = 30^\circ$. ——, present results, ●, experimental results [28].

4. NUMERICAL RESULTS

In order to validate the boundary integral formulation presented above, in this section some comparisons are presented between the present numerical results and experimental data as well as numerical results available in the literature, for subsonic rotors in hover and forward flight.

In the following, N_1, N_2, and N_W define, respectively, the number of discretization elements used chordwise, spanwise and along the wake. Furthermore, N_S is the number of wake spirals used to describe the wake geometry.

4.1. HOVERING ROTORS

For the analysis of subsonic hovering rotors, the configuration analyzed at the DNW under the experimental program within the HELINOISE project has been considered. As reported in reference [28], in that experimental program, the rotor tested is a 40% geometrically and dynamically scaled model of a four-bladed, hingeless BO-105 main rotor. The rotor has a diameter of 4 m with a root cut-out of 0·35 m and a chord length

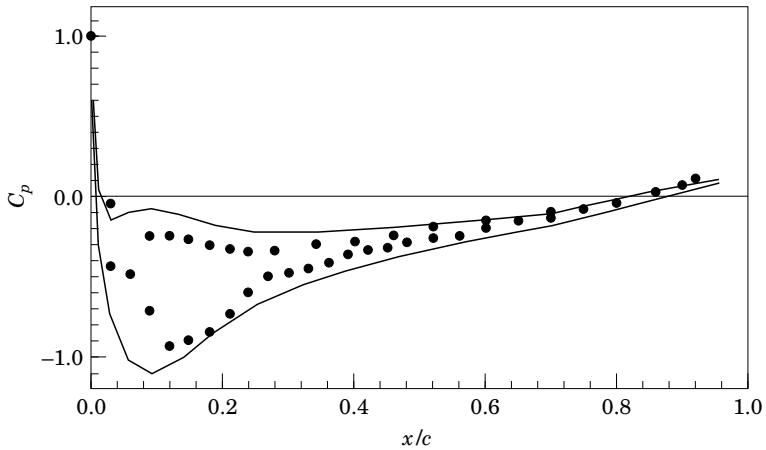

Figure 15. Pressure coefficient at section $r/R = 0{\cdot}97$ of the BO-105 main rotor at azimuthal position $\psi = 120^\circ$. ——, present results, ●, experimental results [28].

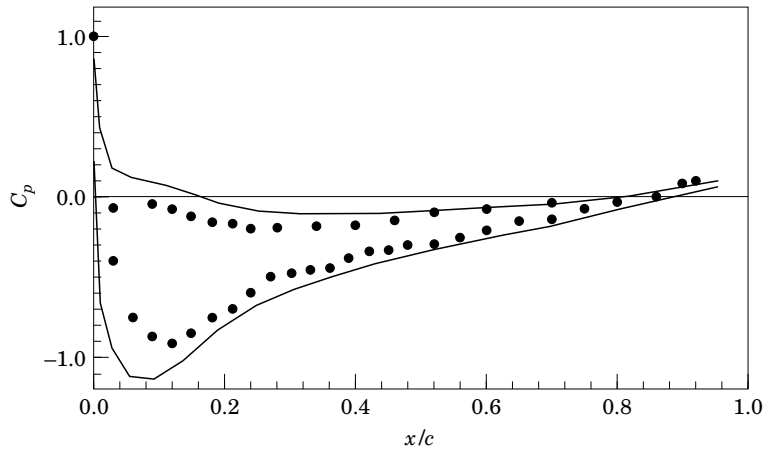

Figure 16. Pressure coefficient at section $r/R = 0{\cdot}97$ of the BO-105 main rotor at azimuthal position $\psi = 210^\circ$. ——, present results, ●, experimental results [28].

of 0·121 m. The blades have -8° of linear twist, with a modified NACA 23012 profile, and a coning angle of $2{\cdot}5^\circ$. The nominal rotor operational speed is 1044 r.p.m. For the hovering configuration the tip Mach number is $M_{TIP} = 0{\cdot}645$. For the numerical aerodynamic analysis the following discretization grid has been employed $N_1 = 20$, $N_2 = 14$, and $N_W = 60$, with $N_S = 5$. In Figures 3 and 4 the pressure distributions computed at the blade sections $r/R = 0{\cdot}75$ and $r/R = 0{\cdot}97$, respectively, are compared with measurements [28]; the truncation of the plots near the trailing edge is due to the fact that the pressure (evaluated according to the finite-difference algorithm discussed above) is available only as shown. The agreement between the numerical results and the experimental data is fairly good. For the same configuration the acoustic signal has also been examined. Specifically, three observer locations have been considered, placed 2·3 m below the rotor disk and located, respectively, at 3·4 m, 4 m, and 4·826 m from the rotor axis. Figures 5, 6 and 7 depict, for the three observer locations, the comparison between the measured acoustic signal and the computed acoustic signatures. In Figure 5, two numerical results are shown: one has been obtained by using a simple helicoidal wake

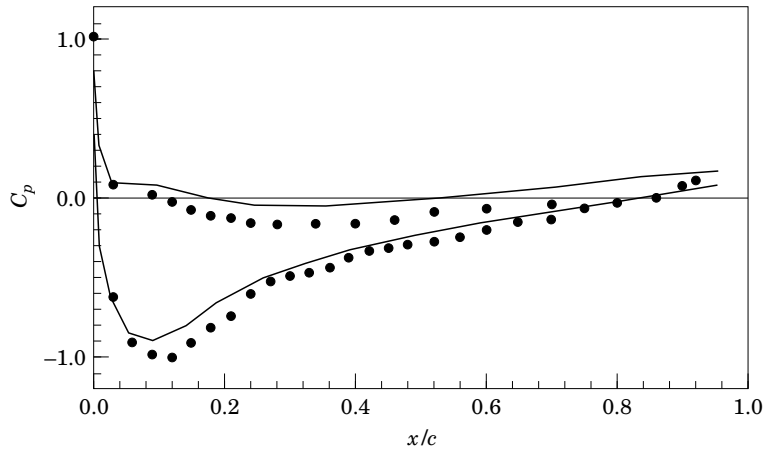

Figure 17. Pressure coefficient at section $r/R = 0{\cdot}97$ of the BO-105 main rotor at azimuthal position $\psi = 300^\circ$. ——, present results, ●, experimental results [28].

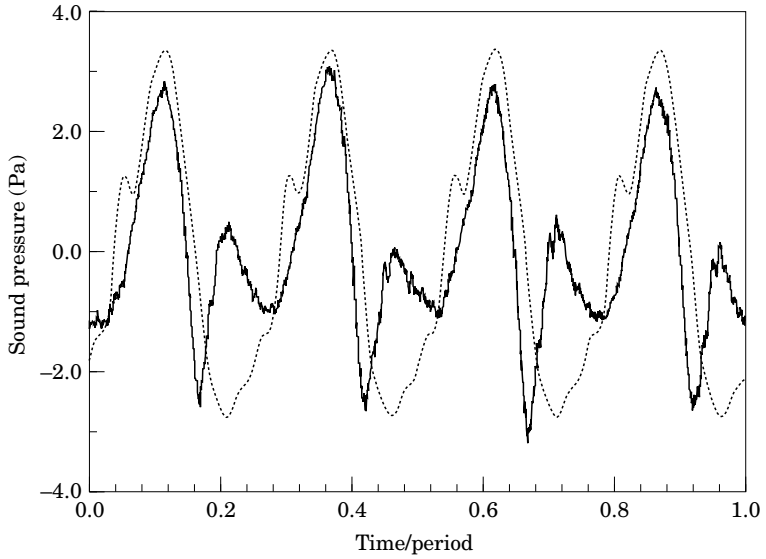

Figure 18. Acoustic signal of the advancing BO-105 main rotor, at observer location $x_W = -4{\cdot}01$ m, $y_W = -2{\cdot}16$ m, $z_W = -2{\cdot}3$ m. - - - - -, present results; ——, experimental results [28].

shape, whereas the other has been obtained (like the rest of the present results concerning hovering configurations) by a wake shape model defined by Landgrebe [29], which is much closer to the actual shape of a hovering rotor wake.

Furthermore, a convergence analysis has been considered. Figure 8 depicts the computed signal at the first observer location (according to the Landgrebe wake model) for the three discretizations corresponding to $N = 2$, $N = 3$, and $N = 4$ (with $N_1 = N_2 = 4N$, $N_W = 20N$ and $N_S = 5$), and the converged result for $N \to \infty$. The latter has been obtained by extrapolating linearly the computed signals. Indeed, Figure 9 (where computed signals

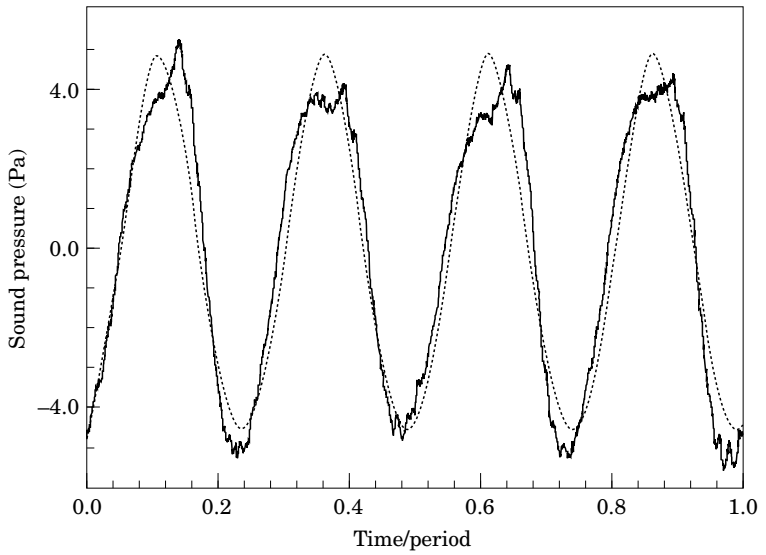

Figure 19. Acoustic signal of the advancing BO-105 main rotor, at observer location $x_W = -2{\cdot}01$ m, $y_W = -2{\cdot}7$ m, $z_W = -2{\cdot}3$ m. - - - - -, present results; ——, experimental results [28].

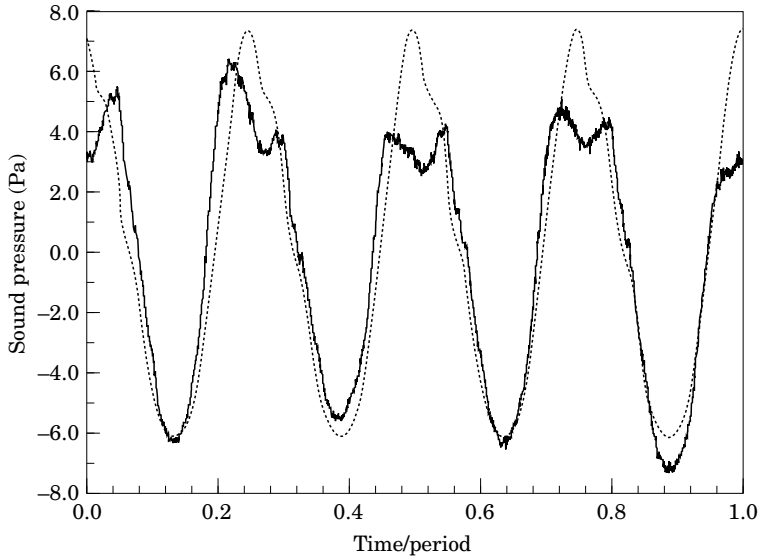

Figure 20. Acoustic signal of the advancing BO-105 main rotor, at observer location $x_W = -2{\cdot}01$ m, $y_W = 0{\cdot}0$ m, $z_W = -2{\cdot}3$ m. - - - - -, present results; ——, experimental results [28].

at three different times are plotted as a function of the inverse of N as defined above) shows a linear convergence rate that yields the converged solution for $1/N = 0$. Note that the acoustic results presented in Figures 5, 6 and 7 for the hovering configuration have to be considered converged solutions obtained by this approach.

Observing the figures described above, it is possible to note the capability of the formulation presented to predict with acceptable accuracy the aerodynamic solution as well as the acoustic one. Furthermore, Figure 5 demonstrates the importance of the wake

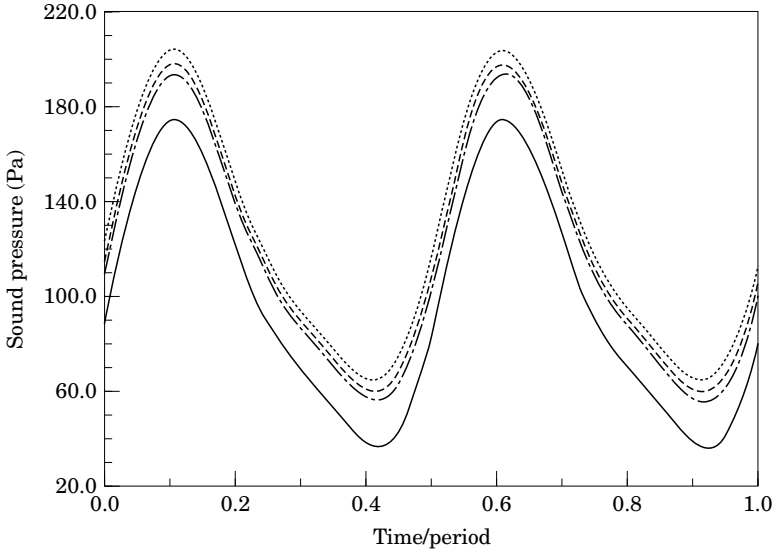

Figure 21. Convergence analysis for the acoustic signal of the advancing UH-1H rotor, at observer location $x_W = 0{\cdot}407$ m, $y_W = -0{\cdot}675$ m, $z_W = -0{\cdot}716$ m. - - - - -, $N = 8$; – – –, $N = 10$; — · — · —, $N = 12$; ——, $N \to \infty$.

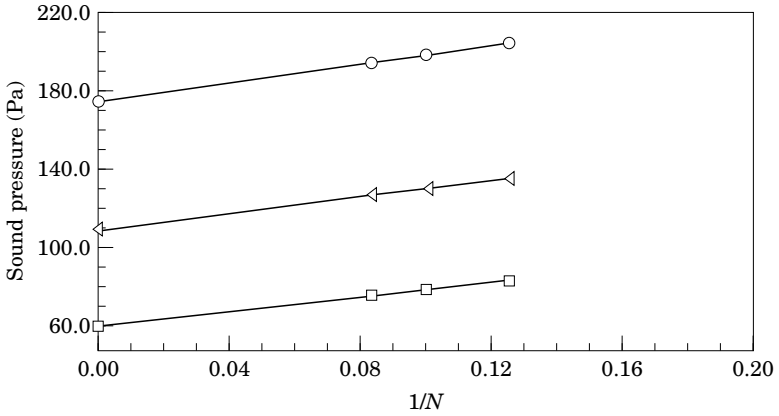

Figure 22. Convergence analysis for the acoustic signal of the advancing UH-1H rotor, at observer location $x_W = 0{\cdot}407$ m, $y_W = -0{\cdot}675$ m, $z_W = -0{\cdot}716$ m. Convergence rate of signals at three different times: ○, time/period = 0·11; ◁, time/period = 0·22; □, time/period = 0·33.

geometry employed in the potential solution in the case of hovering rotors, where the wake generated remains in the vicinity of the rotor, and hence has a strong effect on the aerodynamic field around the blades. Finally, considering the computational cost, note that in order to obtain the results shown in Figures 3 and 4, the CPU time required was of about 20 minutes on an IBM workstation RS 6000 model 360 with a 32Mb RAM.

4.2. ADVANCING ROTORS

For the case of rotors in forward flight, we have analyzed a test case studied in reference [28] as well as one of the cases studied by Brentner [30].

For the problem of the BO-105 main-rotor studied by reference [28] (see the description above) one considers here the case in ascent forward flight, with an effective tip-path-plane angle $\alpha'_{TPP} = -14{\cdot}63^\circ$, advance ratio $\mu = 0{\cdot}148$, hovering hip Mach number $M_{TIP} = 0{\cdot}645$, and feathering motion (see reference [28]). Figures 10, 11, 12 and 13 show the comparison

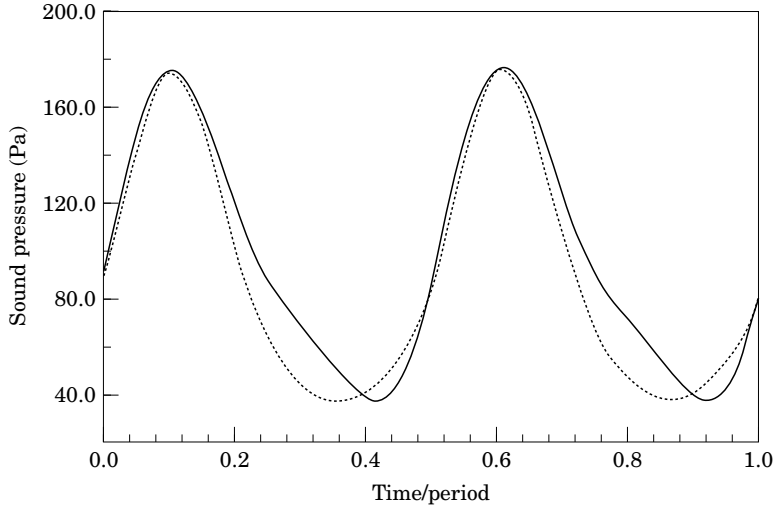

Figure 23. Acoustic signal of the advancing UH-1H rotor, at observer location $x_W = 0{\cdot}407$ m, $y_W = -0{\cdot}675$ m, $z_W = -0{\cdot}716$ m. ——, present results, - - - - -, numerical results of reference [30].

between the measured pressure distributions and those calculated by the present methodology at the radial section $r/R = 0{\cdot}75$, at the blade azimuthal positions $\psi = 30^\circ$, $\psi = 120^\circ$, $\psi = 210^\circ$, and $\psi = 300^\circ$, respectively. The numerical results have been obtained by the following discretization grid: $N_1 = 15$, $N_2 = 16$, and $N_W = 48$, with $N_S = 2$. The agreement between the numerical and the experimental data is satisfactory and is of the same level of accuracy as that presented for the hover test case. This proves the capability of the formulation to capture the unsteady effects in the forward flight configuration that are not present in the hovering one. A similar comparison, for the pressure distribution on the radial section $r/R = 0{\cdot}97$, is illustrated in Figures 14, 15, 16 and 17. Also in this case, the agreement between the experimental data and the numerical results is as satifactory as that obtained in the hover configuration. The simplifying assumption of undeformed wake (introduced in section 3.2) appears to be acceptable for aerodynamic analysis; this is not surprising, since for rotors in ascent forward flight the wake rapidly moves away from the blade and BVI effects on aerodynamics are negligible (as mentioned above, they can be accurately predicted only if a free-wake analysis is performed). Nonetheless, moderate BVI effects are observable in the acoustic signal measurements. Indeed, for the same rotor configuration, the acoustic signal was also computed at three observer positions. In the wind tunnel frame of reference (with co-ordinates denoted by x_W, y_W, z_W, with origin located at the hub and x_W-axis in the direction of undisturbed flow and z_W-axis opposite to the direction of gravity) the first observer is located at $x_W = -4{\cdot}01$ m, $y_W = -2{\cdot}16$ m, $z_W = -2{\cdot}3$ m, the second observer is located at $x_W = -2{\cdot}01$ m, $y_W = -2{\cdot}7$ m, $z_W = -2{\cdot}3$ m, whereas the third one is located at $x_W = -2{\cdot}01$ m, $y_W = 0{\cdot}0$ m, $z_W = -2{\cdot}3$ m. The comparisons between measured acoustic signals and calculated acoustic signals in the positions mentioned above are shown in Figures 18–20, and demonstrate a good agreement for blade-passage frequency signals, whereas higher harmonics (see Figure 18) are not correctly captured; this is to be expected, because the BVI effects (moderately present in this case) cannot be captured with the simple undeformed wake geometry used in this analysis (as mentioned above this requires the use of a free-wake analysis not included in this work).

Finally, one of the forward-flight cases studied by Brentner [30] has been considered. It consists of the articulated UH-1H rotor with an angle of attack of the rotor shaft $\alpha_F = -8^\circ$, advance ratio $\mu = 0{\cdot}124$, and both flapping and feathering motions (see reference [30]). For this configuration a convergence analysis has been performed. Considering the acoustic signal calculated at $x_W = 0{\cdot}407$ m, $y_W = -0{\cdot}675$ m, $z_W = -0{\cdot}716$ m, for $N_1 = N_2 = N$, $N_W = 12N$ and $N_S = 2$, Figures 21 and 22 depict, respectively, time history and convergence rate with $N = 8$, 10, 12, and the converged solution for $N \to \infty$. Similarly to the hovering-case analysis, the rate of convergence is linear as well, and converged results are obtained by a linear extrapolation law. These are compared in Figure 23 with the acoustic-pressure time history computed by Brentner [30]. The two numerical results appear to be in a good agreement, confirming the capability of the presented formulation to capture the aerodynamic/aeroacoustic solution for rotors in forward flight.

5. CONCLUDING REMARKS

A boundary integral formulation for the unified aerodynamic and aeroacoustic analysis of rigid lifting bodies in arbitrary motion has been presented.

Numerical results concerning hovering and advancing rotor configurations have been presented in order to demonstrate the capability of the methodology to capture aerodynamic and aeroacoustic solutions. For subsonic-flow rotors in hover and forward

flight, the comparison with existing numerical results and available experimental data has shown a satisfactory agreement for both the aerodynamic and the aeroacoustic solutions.

As noted above, a considerable improvement in the results is obtained by using the Landgrebe [29] wake geometry, instead of the helicoidal one. It appears desirable to use a wake geometry obtained from a free-wake analysis. Such a methodology is not available for compressible flows (although the wake geometry obtained from the incompressible free-wake analysis of reference [17] could be used on the basis of the experimental results showing that the wake geometry is not strongly affected by the compressibility). Also, the use of a wake geometry from a free-wake analysis appears essential for advancing rotor configurations with lower values of the tip-path-plane angle, where the wake and the rotor are very close (BVI problem). Indeed, an accurate prediction of the wake vorticity location is the main feature in a BVI analysis, and may be determined by the present formulation considering the wake shape as part of the solution (free-wake analysis, see reference [17]). This work is currently under development, along with that on transonic flows for hover and forward flight where the contribution of non-linear terms becomes essential and generates the characteristic high-speed impulsive noise.

ACKNOWLEDGMENTS

The aerodynamic activity reported in this work has been partially supported through a grant by Agusta S.p.A. to the University of Rome III and by the project HELISHAPE within the BRITE EURAM program.

REFERENCES

1. J. E. Ffowcs Williams and D. L. Hawkings 1969 *Philosophical Transactions of the Royal Society* **A264**, 321–342. Sound generated by turbulence and surfaces in arbitrary motion.
2. F. Farassat 1980 *American Institute of Aeronautics and Astronautics Journal* **19**, 1122–1130. Linear acoustic formulas for calculation of rotating blade noise.
3. F. Farassat 1994 *NASA TP*-3428. Introduction to generalized functions with applications in aerodynamics and aeroacoustics.
4. A. S. Lyrintzis 1994 *Journal of Fluids Engineering* **116**, 665–676. Review: the use of Kirchhoff's method in computational aeroacoustics.
5. F. Farassat and M. K. Myers 1988 *Journal of Sound and Vibration* **123**, 451–460. Extension of Kirchhoff's formula to radiation from moving surfaces.
6. D. B. Hanson 1983 *American Institute of Aeronautics and Astronautics Journal* **21**, 881–889. Compressible helicoidal surface theory for propeller aerodynamics and noise.
7. D. B. Hanson 1991 *NASA CR*-4329. Unified aeroacoustic analysis for high speed turboprop aerodynamics and noise.
8. L. N. Long 1983 *American Institute of Aeronautics and Astronautics Paper* 83–1821. The aerodynamics and propellers and rotors using an acoustic formulation in the time domain.
9. L. N. Long and G. A. Watts 1987 *American Institute of Aeronautics and Astronautics Journal* **25**, 1442–1448. Arbitrary motion aerodynamics using an aeroacoustic approach.
10. F. Farassat 1984 *American Institute of Aeronautics and Astronautics Journal* **22**, 1337–1340. A new aerodynamic integral equation based on an acoustic formula in the time domain.
11. F. Farassat 1985 *AGARD CP*-366. Theoretical analysis of linearized acoustics and aerodynamics of advanced supersonic propellers.
12. F. Farassat and M. K. Myers 1986 *American Institute of Aeronautics and Astronautics Paper* 86–1877. Aerodynamics via acoustics: application of acoustic formulas for aerodynamic calculations.
13. L. Morino 1974 *NASA CR*-2464. A general theory of unsteady compressible potential aerodynamics.
14. L. Morino and K. Tseng 1990 in *Boundary Element Methods in Nonlinear Fluid Dynamics* (editors P. K. Banerjee and L. Morino), *Developments in Boundary Element Methods* **6**; Barking,

U.K: Elsevier Applied Science Publishers; 183–245. A general theory of unsteady compressible potential flows with applications to airplanes and rotors.
15. L. Morino and M. Gennaretti 1992 in *Computational Nonlinear Mechanics in Aerospace Engineering* (editor S. N. Atluri), *AIAA Progress in Aeronautics and Astronautics* **146**, Washington, DC: AIAA; 279–321. Boundary integral equation methods for aerodynamics.
16. L. Morino 1993 *Applied Mechanics Reviews* **46**, 445–466. Boundary integral equations in aerodynamics.
17. L. Morino, B. K. Bharadvaj, M. I. Freedman and K. Tseng 1989 *Computational Mechanics* **4**, 231–243. Boundary integral equation for wave equation with moving boundary and applications to compressible aerodynamics of airplanes and helicopters.
18. M. Gennaretti 1989 *Tesi di Laurea*, *University of Rome* '*La Sapienza*', *Rome*, *Italy* (in Italian). Metodo delle Equazioni Integrali al Contorno per Analisi Aerodinamica e Aeroacustica di Rotori in Flussi Potenziali, Compressibili, Non Stazionari.
19. M. Gennaretti and L. Morino 1990 in *Boundary Element Methods in Engineering* (editors B. S. Annigeri and K. Tseng); Heidelberg: Springer Verlag; 515–528. A unified approach for aerodynamics and aeroacoustics of rotors in compressible potential flows.
20. M. Gennaretti and L. Morino 1992 *Aeronautical Journal* **96**, 15–19. A boundary element method for the potential, compressible aerodynamics of bodies in arbitrary motion.
21. L. Morino and M. Gennaretti 1992 *American Institute of Aeronautics and Astronautics Paper* 92–02003. Toward an integration of aerodynamics and aeroacoustics of rotors.
22. M. Gennaretti 1993 *Doctoral Thesis*, *University of Rome* '*La Sapienza*', *Rome*, *Italy* (in Italian). Una Formulazione Integrale di Contorno per la Trattazione Unificata di Flussi Aeronautici Viscosi e Potenziali.
23. K. S. Brentner and F. Farassat 1994 *Journal of Sound and Vibration* **170**, 79–96. Helicopter noise prediction: the current status and future direction.
24. M. J. Lighthill 1952 *Proceedings of the Royal Society* **A11**, 564–587. On sound generated aerodynamically, I: General theory.
25. M. Gennaretti, U. Iemma and L. Morino 1994 *AGARD CP*-522. Method for unified transonic aerodynamic and aeroacoustic analysis of hovering rotors.
26. A. J. Chorin and J. E. Marsden 1990 *A Mathematical Introduction to Fluid Mechanics*. Heidelberg: Springer Verlag.
27. M. J. Lighthill 1958 *Journal of Fluid Mechanics* **4**, 383–392. On displacement thickness.
28. W. R. Splettstoesser, B. Junker, K.-J. Schultz, W. Wagner, W. Weitemeyer, A. Protopsaltis and D. Fertis 1993 *DLR-Mitt* 93–09. The HELINOISE aeroacoustic rotor test in the DNW—test documentation and representative results.
29. A. J. Landgrebe 1971 *USAAMRDL TR*-71–24. An analytical and experimental investigation of helicopter rotor hover performance and wake geometry characteristics.
30. K. S. Brentner 1986 *NASA TM*-87721. Prediction of helicopter rotor discrete frequency noise.